SAND2019-10667J

A Graphical Design Approach for Two-Input Single-Output Systems Exploiting Plant/Controller Alignment: Design and Application

Nathan A. Weir*
Principal Member of Technical Staff
Sandia National Laboratories
Albuquerque, NM 87185
naweir@sandia.gov

Andrew G. Alleyne
Professor, Fellow of ASME
Department of Mechanical Science and Engineering
University of Illinois at Urbana-Champaign
Urbana, IL 61801
alleyne@illinois.edu

ABSTRACT

Due to the unique structure of two-input single-output (TISO) feedback systems, several closed loop properties can be characterized using the concepts of plant and controller "directions" and "alignment". Poor plant/controller alignment indicates significant limitations in terms of closed loop performance. In general, it is desirable to design a controller that is well aligned with the plant in order to minimize the size of the closed loop sensitivity functions and closed loop interactions. Although the concept of alignment can be a useful analysis tool for a given plant/controller pair, it is not obvious how a controller should be designed to achieve good alignment. We present a new controller design approach, based on the PQ method [1], which explicitly incorporates knowledge of alignment into the design process. This is accomplished by providing graphical information about the alignment angle on the Bode plot of the PQ frequency response. We show the utility of this approach through a design example.

1 INTRODUCTION

Two-input single-output (TISO) feedback systems are commonly found in a variety of practical applications which involve two actuators that act together in parallel to produce a desired output. These are

*Corresponding author.

Sandia National Laboratories is a multimission laboratory managed and operated by National Technology & Engineering Solutions of Sandia, LLC, a wholly owned subsidiary of Honeywell International Inc., for the U.S. Department of Energy's National Nuclear Security Administration under contract DE-NA0003525.

sometimes referred to as dual-stage or coarse/fine control systems. Examples include nano-positioning systems [2], data storage systems such as dual-stage tape drives [3] and dual-stage hard disk drive (HDD) servos [1], optical instruments such as interferometers [4] and fast steering mirrors [5], manufacturing applications such as wafer stage control [6], and automotive applications like engine throttle control [7] and vehicle steering control [8].

Given the unique structure of TISO feedback systems, several closed loop properties and performance limitations can be characterized using the concepts of plant and controller "directions" and "alignment" [9]. Poor plant/controller alignment indicates significant limitations in terms of closed loop performance. In general, it is desirable to design a controller that is well aligned with the plant in order to minimize the size of the closed loop sensitivity functions and closed loop interactions at the plant input. Although the concept of alignment can be a useful analysis tool for a given plant/controller pair (e.g., see [10,11]), it is not entirely clear how a controller should be designed to achieve good alignment with a particular plant over frequency.

A decentralized control design procedure which exploits alignment is developed in [12], however, is only applicable to ill-conditioned two-input two-output (TITO) systems. This paper presents a new approach which incorporates knowledge of the alignment explicitly into the controller design process for TISO feedback systems. We use the well-known PQ method [1] as the basis of this approach as it is particularly well suited to fit within the alignment framework presented in [9].

The remainder of the paper is organized as follows. Section 2 describes the TISO feedback system configuration and the relevant transfer functions that dictate closed loop performance. Section 3 introduces the concept of plant/controller alignment and describes its relationship to various closed loop properties of the TISO feedback configuration. Section 4 summarizes TISO controller design using the PQ method and introduces a new graphical approach that explicitly accounts for plant/controller alignment. The utility of this approach is highlighted through a design example in Section 5. Simulated and experimental results are given in Sections 6 and 7, respectively. Section 8 contains concluding remarks.

2 TISO FEEDBACK SYSTEMS

The TISO unity feedback configuration is depicted in Fig. 1, where

$$G(s) = \begin{bmatrix} g_1(s) & g_2(s) \end{bmatrix} \quad \text{and} \quad C(s) = \begin{bmatrix} c_1(s) \\ c_2(s) \end{bmatrix} \tag{1}$$

are the plant and controller transfer matrices, respectively, with $G(s) \in \mathbb{C}^{1\times 2}$ and $C(s) \in \mathbb{C}^{2\times 1}$; $r \in \mathbb{R}$ is the reference input, $y \in \mathbb{R}$ is the system output, $e \in \mathbb{R}$ is the measured error signal, $u_1 \in \mathbb{R}$ and $u_2 \in \mathbb{R}$ are the control inputs, $n \in \mathbb{R}$ is the measurement noise, $d_{i1} \in \mathbb{R}$ and $d_{i2} \in \mathbb{R}$ are the input disturbances, and $d_o \in \mathbb{R}$ is the output disturbance.

Omitting the dependence on the frequency variable $s = j\omega$ to simplify notation, it is convenient to define the input and output loop transfer functions as

$$L_I \coloneqq CG \quad \text{and} \quad L_O \coloneqq GC \tag{2}$$

where $L_I \in \mathbb{C}^{2\times 2}$ is obtained from breaking the loop at the input of the plant and $L_O \in \mathbb{C}$ is obtained from breaking the loop at the output of the plant. The input sensitivity and complementary sensitivity functions

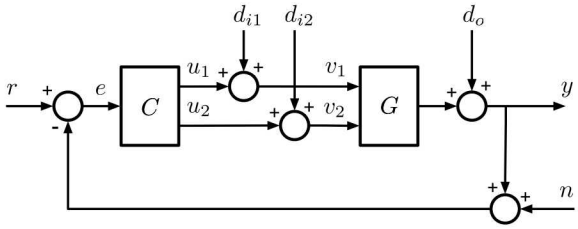

Fig. 1 TISO feedback system

are then defined as

$$S_I \coloneqq (I + L_I)^{-1} \quad \text{and} \quad T_I \coloneqq L_I(I + L_I)^{-1} \tag{3}$$

where $S_I \in \mathbb{C}^{2\times 2}$ and $T_I \in \mathbb{C}^{2\times 2}$ must satisfy the identity $S_I + T_I = I$. Similarly, the output sensitivity and complementary sensitivity functions are defined as

$$S_O \coloneqq (1 + L_O)^{-1} \quad \text{and} \quad T_O \coloneqq L_O(1 + L_O)^{-1} \tag{4}$$

where $S_O \in \mathbb{C}$ and $T_O \in \mathbb{C}$ must satisfy the identity $S_O + T_O = 1$.

We assume that the closed loop system is internally stable and write the closed loop response of the system to exogenous inputs as

$$Y = T_O\,(R - N) + S_O D_O + S_O G D_I \tag{5}$$
$$E = S_O\,(R - D_O - N) - S_O G D_I \tag{6}$$
$$U = S_I C\,(R - D_O - N) - T_I D_I \tag{7}$$
$$V = S_I C\,(R - D_O - N) + S_I D_I \tag{8}$$

For the TISO feedback configuration, we see that the output sensitivity and complementary sensitivity functions are scalar valued. As is the case for single-input single-output (SISO) feedback, it follows from Eq. (4) that the use of high gain feedback such that $|L_O| \to \infty$ will force $|T_O| \to 1$ and $|S_O| \to 0$. Thus, at frequencies where high gain can be employed, it follows from Eqs. (5) and (6) that good reference tracking and disturbance rejection can be achieved at the plant output.

On the other hand, the high gain properties at the plant input are not as simple. In general, $S_I \neq S_O$ unless G and C commute (e.g., as in the SISO case). For the TISO feedback configuration, S_I and S_O do not even have the same dimensions. Hence, "small" S_O does not necessarily imply "small" S_I; in other words, good performance at the plant output does not necessarily indicate good performance at the plant input [13]. Indeed, even for systems that achieve reasonable performance at the plant output, very poor performance at the plant input may result from an inappropriate choice of C.

In this paper, we primarily focus on the input properties of the TISO feedback configuration which are dictated by Eqs. (7) and (8) through the input sensitivity functions S_I, T_I, and $S_I C$. We adopt the framework presented in [9] which introduces the concepts of plant and controller directions and alignment.

These concepts are used to describe the relationship between the open and closed loop properties of the TISO feedback configuration. The relevant concepts and associated properties of [9] are summarized in the following section.

3 TISO FEEDBACK PROPERTIES

3.1 Plant/controller directions and alignment

The plant and controller transfer matrices given in Eq. (1) can be viewed as complex row and column vectors, respectively. Thus, it is useful to define the *plant direction* at frequency ω as the row space of the plant, $\mathcal{R}_{\text{row}}(G(j\omega))$. Likewise, define the *controller direction* at frequency ω as the column space of the controller, $\mathcal{R}(C(j\omega))$. The *alignment angle* between the plant and controller at frequency ω is then defined as [9]

$$\phi(j\omega) \coloneqq \arccos\left(\frac{|G(j\omega)C(j\omega)|}{\|G(j\omega)\|\|C(j\omega)\|}\right) \tag{9}$$

where $\|\cdot\|$ is the standard vector 2-norm and, by definition, $\phi(j\omega) \in [0^\circ, 90^\circ]$. We say that the controller and plant are *perfectly aligned* if $\phi(j\omega) = 0^\circ$ and *completely misaligned* if $\phi(j\omega) = 90^\circ$. Furthermore, we say that the plant and controller are *well aligned* if $\phi(j\omega) \approx 0^\circ$ and *poorly aligned* if $\phi(j\omega) \approx 90^\circ$.

3.2 Alignment and input response

For the TISO feedback configuration, the size of the input sensitivity and complementary sensitivity is determined by the plant/controller alignment. Omitting the dependence on the frequency variable $s = j\omega$, bounds on the size of the input sensitivity and complementary sensitivity can be expressed as [9]

$$\|S_I\| \leq \sqrt{1 + |T_O|^2 \tan^2\phi} + |S_O| \tag{10}$$

$$\|S_I\| \leq \max\{1, |S_O|\} + |T_O| \tan\phi \tag{11}$$

$$\|S_I\| \geq \max\{\sqrt{1 + |T_O|^2 \tan^2\phi}, |S_O|\} \tag{12}$$

$$\|T_I\| = \frac{|T_O|}{\cos\phi} \tag{13}$$

$$\|S_I C\| = \frac{|T_O|}{\|G\|\cos\phi} \tag{14}$$

where $\|\cdot\|$ denotes the induced matrix norm (i.e., maximum singular value) in Eqs. (10)–(13) and the standard vector 2-norm in Eq. (14). Using high gain feedback such that $|L_O| \to \infty$, $|S_O| \to 0$, and $|T_O| \to 1$,

it follows from Eqs. (10), (12), (13), and (14) that

$$\|S_I\| \to \frac{1}{\cos\phi} \tag{15}$$

$$\|T_I\| \to \frac{1}{\cos\phi} \tag{16}$$

$$\|S_I C\| \to \frac{1}{\|G\|\cos\phi} \tag{17}$$

Equations (15)–(17) imply that the use of high gain at frequencies where alignment is poor (i.e., as $\phi \to 90^\circ$) forces $\|S_I\|$, $\|T_I\|$, and potentially $\|S_I C\|$ to be very large. In practice, this means that if the size of $\|S_I\|$, $\|T_I\|$, or $\|S_I C\|$ is unacceptable, it will be necessary to use lower gain and/or achieve better plant/controller alignment. This presents a tradeoff between output performance (which requires high gain so that $|S_O|$ is small) and input performance (which requires lower gain and/or better alignment so that $\|S_I\|$ or $\|T_I\|$ is not too large).

3.3 Alignment and closed loop interactions

For the TISO feedback configuration, the closed loop interactions at the plant input are also determined by the plant/controller alignment. The off-diagonal elements of T_I satisfy the bounds [9]

$$|T_{I12}| + |T_{I21}| \geq |T_O| \tan\phi \tag{18}$$

$$|T_{Iij}| \leq \frac{|T_O|}{\cos\phi}\left(1 + \left|\frac{g_i}{g_j}\right|^2\right)^{-1/2} \quad \text{for } i \neq j \tag{19}$$

where g_i and g_j are the elements of the plant transfer matrix given in Eq. (1).

Equation (18) implies that the use of high gain at frequencies where alignment is poor (i.e., as $\phi \to 90^\circ$) forces one or both of the off-diagonal elements of T_I to be very large. Likewise, the corresponding off-diagonal elements of S_I will also be very large according to the identity $S_I + T_I = I$. Thus, the closed loop response will necessarily exhibit strong interactions at the plant input. In practice, this means that a disturbance at the first input to the plant, d_{i1}, will potentially result in a very large response at the second output of the controller, u_2 (and vice-versa). This can be problematic, especially if the secondary actuator saturates at a relatively low level. If this is undesirable, it will be necessary to use lower gain and/or achieve better plant/controller alignment.

3.4 Perfect alignment

We now show that perfectly aligned controllers have special properties. Consider the case where the controller is perfectly aligned with the plant (i.e., $\phi = 0^\circ$). It follows from Eqs. (11)–(14) that perfect

alignment minimizes the sizes of the input sensitivity functions, yielding

$$\|S_I\| = \max\{1, |S_O|\} \tag{20}$$

$$\|T_I\| = |T_O| \tag{21}$$

$$\|S_I C\| = \frac{|T_O|}{\|G\|} \tag{22}$$

Similarly, it follows from Eqs. (18) and (19) that perfect alignment minimizes the closed loop interactions at the plant input. Note, however, that perfect alignment does not necessarily reduce the level of interaction to zero, but to the minimum possible level dictated by the plant. The minimum possible interactions are given by [9]

$$|T_{I12}| = |T_{I21}| = |T_O| \frac{|g_1||g_2|}{|g_1|^2 + |g_2|^2} \tag{23}$$

where g_1 and g_2 are the elements of the plant transfer matrix given in Eq. (1).

Although the above results indicate that the controller should be well aligned with the plant at all frequencies, this interpretation must be viewed with caution. As noted in [14], requiring perfect alignment at all frequencies can introduce non-minimum phase (NMP) zeros into the open loop transfer function if the plant direction varies with frequency. These unstable zeros can limit the achievable closed loop bandwidth of the system [15]. Fortunately, perfect alignment is not necessary to achieve satisfactory performance.

So then, how much misalignment is acceptable? It is shown in [9] that closed loop performance is relatively insensitive to moderate deviations from $\phi = 0^\circ$, and that the closed loop response is insensitive to alignment at frequencies for which the gain is sufficiently small (i.e., outside the closed loop bandwidth). Using Eq. (13) to demonstrate this insensitivity, we have

$$\begin{aligned} \phi = 25^\circ \quad &\Longrightarrow \quad \|T_I\| = 1.1\,|T_O| \\ \phi = 45^\circ \quad &\Longrightarrow \quad \|T_I\| = 1.4\,|T_O| \\ \phi = 60^\circ \quad &\Longrightarrow \quad \|T_I\| = 2.0\,|T_O| \end{aligned}$$

Thus, perfect alignment is not necessary to achieve reasonable performance. The alignment angle is a more useful indicator of poor performance when alignment is poor. Ultimately, it is important to avoid poor alignment, but it is not necessary to demand perfect alignment over all frequencies.

4 TISO CONTROLLER DESIGN

In the previous section, we showed how plant/controller alignment relates to various closed loop properties of the TISO feedback configuration. In general, it is desirable to design a well aligned controller to minimize the size of the input sensitivity functions and closed loop interactions at the plant input. Although it is straightforward to evaluate the alignment angle over frequency using Eq. (9) for a given plant/controller pair, it is not entirely clear how a controller should be designed to achieve good alignment with a particular plant. Thus, it would be beneficial to include knowledge of alignment in the controller design process itself. In this section, we introduce a new approach which incorporates knowledge of the alignment explicitly into

the controller design process. We use the well-known PQ method [1] as the basis of this approach as it is well suited to fit within the framework discussed in Sec. 3. The PQ design procedure is briefly summarized below.

4.1 PQ method

The PQ method [1] is a straightforward controller design technique which transforms the TISO feedback problem into two individual SISO design problems as depicted in Fig. 2. This is accomplished by splitting the controller into pre- and post-compensation parts such that

$$C(s) \coloneqq c_0(s) \begin{bmatrix} c_1'(s) \\ c_2'(s) \end{bmatrix} \tag{24}$$

where $c_1'(s)$ and $c_2'(s)$ are the pre-compensator elements, and $c_0(s)$ is the post-compensator. The PQ method consists of two primary steps. The first step involves the construction of the G_{SISO} subsystem shown in Fig. 2(b), also known as "squaring down" the plant [16]. The second step designs a feedback controller, $c_0(s)$, for the G_{SISO} subsystem which satisfies stability and performance requirements. The pre-compensators, $c_1'(s)$ and $c_2'(s)$, are simultaneously selected to obtain G_{SISO} such that the following conditions are satisfied:

1. Ensure G_{SISO} is minimum phase to avoid inherent bandwidth limitations. The parallel combination G_{SISO} can become non-minimum phase even when $c_1'(s)g_1(s)$ and $c_2'(s)g_2(s)$ are both individually minimum phase [17].
2. Ensure the relative output contribution of each path is appropriately allocated over frequency. Often, parallel actuators are selected to perform better in different frequency ranges.
3. Minimize destructive interference due to relative phase lag between paths. Interference occurs when two actuators effectively cancel each other to yield a net output near zero.

To assist with the selection of $c_1'(s)$ and $c_2'(s)$ which satisfy the above conditions, a fictitious "PQ" feedback system is constructed as follows. The zeros of G_{SISO} can be expressed as the solution to the equation

$$G_{\text{SISO}}(s) = c_1'(s)g_1(s) + c_2'(s)g_2(s) = 0 \tag{25}$$

The *plant ratio* and *controller ratio* are defined as

$$P(s) \coloneqq \frac{g_1(s)}{g_2(s)} \quad \text{and} \quad Q(s) \coloneqq \frac{c_1(s)}{c_2(s)} = \frac{c_1'(s)}{c_2'(s)}, \tag{26}$$

respectively. Rearranging Eq. (25), we can write

$$1 + \frac{g_1(s)c_1'(s)}{g_2(s)c_2'(s)} = 1 + P(s)Q(s) = 0 \tag{27}$$

Equation (27) represents the characteristic equation of the PQ feedback system depicted in Fig. 3. The closed loop poles of the PQ feedback system are the zeros of G_{SISO}. Thus, selecting Q to stabilize the

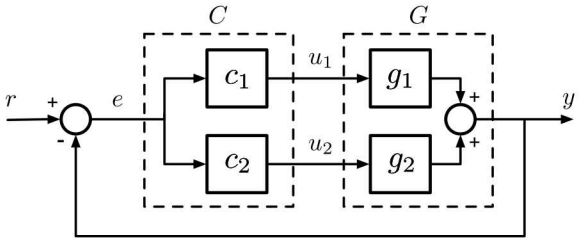

(a) TISO feedback system

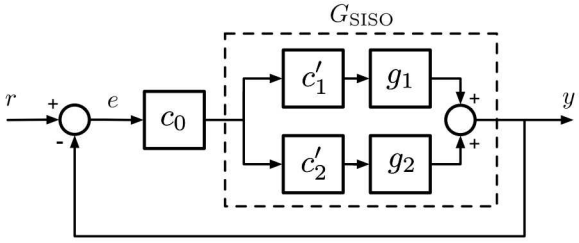

(b) SISO equivalent system

Fig. 2 PQ equivalent representation

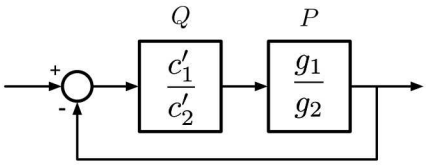

Fig. 3 PQ feedback system

PQ feedback system ensures that G_{SISO} will have stable (i.e., minimum phase) zeros, thereby satisfying condition #1. The magnitude of PQ determines the relative contributions of the parallel paths as a function of frequency. The 0 dB crossover of $|PQ|$ is the *hand-off frequency* at which the parallel paths contribute equally, and can be selected via proper tuning of Q to satisfy condition #2. The phase of PQ determines the relative stability of the zeros of G_{SISO} and also dictates the amount of destructive interference which occurs between the parallel subsystems. Destructive interference can be avoided by selecting the phase margin to be greater than 60 degrees [1], thus satisfying condition #3. Frequency domain techniques are well suited for the design of Q, which effectively transforms the selection of pre-compensators c_1' and c_2' into a PQ loop shaping exercise as depicted in Fig. 4.

A significant disadvantage of the PQ method is that it does not explicitly take into account closed loop performance at the plant input. This is a direct result of treating the TISO feedback problem as two separate SISO problems. In fact, the input response of the TISO feedback system becomes completely masked in the formation of G_{SISO} as shown in Fig. 2(b). Furthermore, the PQ method provides no insight into system performance limitations with respect to plant/controller alignment as described in Sec. 3. Clearly, the selection of Q (and hence c_1' and c_2') will directly influence plant/controller alignment. However, the relationship between alignment and the PQ loop shape is nonintuitive. In the following section, we describe a new approach that augments the PQ design procedure with additional information regarding plant/controller

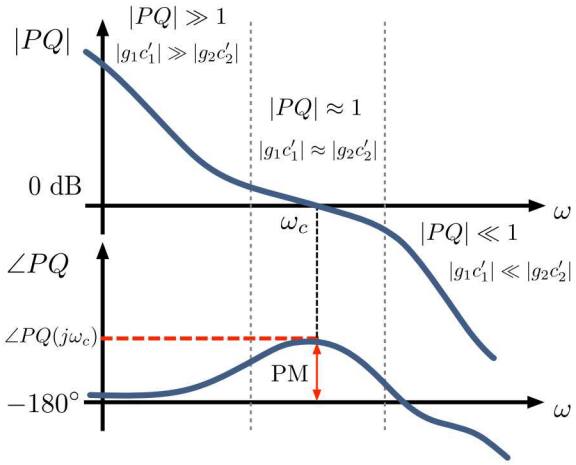

Fig. 4 PQ Bode plot

alignment so that the designer can make well-informed choices (from the perspective of input response) when shaping the PQ feedback loop.

4.2 Alignment contours

To incorporate alignment into the PQ loop shaping process, we modify the conventional Bode plot by adding magnitude and phase contours which represent specific values of the plant/controller alignment angle over frequency. The intersection of the PQ magnitude and phase responses with these contours indicate frequencies at which the alignment angle reaches a particular value. This allows the designer to easily determine the alignment over frequency for a given PQ loop shape. More importantly, the contours provide additional guidelines in the loop shaping process. This is similar to the Bode sensitivity and robustness contours developed in [18–21]. However, in the context of plant/controller alignment, the contours are used on the Bode plot of the PQ loop shape instead of the open loop transfer function.

To derive the magnitude and phase contours, we start with the definition of the plant/controller alignment angle given by Eq. (9) and expand in terms of the plant and controller ratios

$$\begin{aligned}\cos\phi &= \frac{|GC|}{\|C\|\|G\|} \\ &= \frac{|g_1c_1 + g_2c_2|}{\sqrt{|c_1|^2+|c_2|^2}\sqrt{|g_1|^2+|g_2|^2}} \\ &= \frac{|1+PQ|}{\sqrt{1+|P|^2+|Q|^2+|PQ|^2}}\end{aligned} \tag{28}$$

where P and Q are the plant and controller ratios defined by Eq. (26). Squaring both sides of Eq. (28) and

expanding, we can write

$$\begin{aligned}\left(1+|P|^2+|Q|^2+|PQ|^2\right)\cos^2\phi &= |1+PQ|^2\\ &= (1+PQ)\left(1+\overline{PQ}\right)\\ &= 1+|PQ|\left(e^{j(\angle P+\angle Q)}+e^{-j(\angle P+\angle Q)}\right)+|PQ|^2\\ &= 1+2\cos\left(\angle PQ\right)|PQ|+|PQ|^2\end{aligned} \tag{29}$$

Rearranging Eq. (29), we obtain a quadratic equation in terms of $|PQ|$

$$\left(\frac{\cos^2\phi}{|P|^2}+\cos^2\phi-1\right)|PQ|^2-2\cos\left(\angle PQ\right)|PQ|+\left(|P|^2\cos^2\phi+\cos^2\phi-1\right)=0 \tag{30}$$

The solutions to this quadratic equation relate the magnitude and phase of the plant and controller ratios required to achieve a given alignment angle. Note that the values of $|PQ|$ and $\angle PQ$ at a particular frequency can be taken directly from the PQ Bode plot.

Using the quadratic formula, we can solve Eq. (30) for the magnitude contour in terms of the phase of the plant and controller ratios and the alignment angle. The magnitude contour is then defined as

$$\begin{aligned}M_a(j\omega,\phi) \coloneqq \frac{1}{|P|^{-2}\cos^2\phi+\cos^2\phi-1}\Bigg[&\cos\left(\angle PQ\right)\\ &\pm\Big\{\cos^2(\angle PQ)-\left(|P|^{-2}\cos^2\phi+\cos^2\phi-1\right)\\ &\qquad\times\left(|P|^2\cos^2\phi+\cos^2\phi-1\right)\Big\}^{\frac{1}{2}}\Bigg]\end{aligned} \tag{31}$$

The solutions given by Eq. (31) are only valid for non-negative real values. Thus, any negative real or complex solutions are discarded. It is useful to plot contours for several different values of the alignment angle in fixed intervals between 0° and 90°, $\phi_k=(k-1)\,\Delta\phi$ for $k=1,2,\ldots,n$; where $\Delta\phi=90^\circ/(n-1)$ and n is the number of contour levels. The intersections between $|P(j\omega)Q(j\omega)|$ and $M_a(j\omega,\phi_k)$ on the Bode magnitude plot are the frequencies for which $\phi=\phi_k$. Note that $M_a(j\omega,\phi_k)$ does not depend on $|PQ|$, thus shifting the magnitude of PQ with a constant gain does not affect the magnitude contours. As a result, it is easy to see how changing the PQ loop gain will affect the alignment angle over frequency.

Similarly, the phase contour can be determined by solving Eq. (30) for phase in terms of the magnitudes of the plant and controller ratios and the alignment angle. The phase contour is then defined as

$$\Phi_a(j\omega,\phi) \coloneqq \arccos\left[\frac{1}{2|PQ|}\left\{\left(\frac{\cos^2\phi}{|P|^2}+\cos^2\phi-1\right)|PQ|^2+|P|^2\cos^2\phi+\cos^2\phi-1\right\}\right] \tag{32}$$

where Φ_a is only valid when the solution to Eq. (32) is real-valued. The intersections between $\angle P(j\omega)Q(j\omega)$ and $\Phi_a(j\omega,\phi_k)$ on the Bode phase plot are the frequencies for which $\phi=\phi_k$. In the following section, we

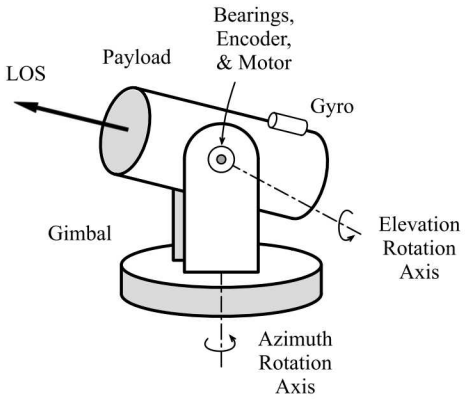

Fig. 5 Gimbaled pointing system

present a design example which shows the utility of the magnitude and phase contours on the PQ Bode plot.

5 DESIGN EXAMPLE: HYBRID FLEXURE BEARING

Gimbaled pointing systems are commonly used to aim and stabilize sensitive instrument payloads such as radars, lasers, cameras, and other electro-optical sensors for a variety of different applications [22]. A typical two-axis gimbal, depicted in Fig. 5, provides the ability to 1) point the payload in a desired direction over a large field of regard, and 2) stabilize the payload line of sight (LOS) in the presence of base disturbances due to host vehicle motion. Typically, the gimbal is suspended by conventional ball bearing joints. Although this allows for a large range of motion, bearing friction can adversely affect the overall system performance.

The following design example is motivated by a hybrid flexure bearing concept which was developed to reduce the effects of friction that degrade performance in systems with ball bearing joints [23–27]. The hybrid flexure bearing, depicted in Fig. 6, combines the large travel advantage of a conventional ball bearing joint with the smooth frictionless motion of a rotational flexure. Incorporating the flexure provides an additional degree of freedom in the system which allows for independent actuation of both the ball bearing inner race and the relative rotation of the flexure.

5.1 Experimental testbed

A single-axis experimental testbed, depicted in Fig. 7, is used to evaluate the performance of the prototype hybrid flexure bearing. The testbed hardware represents a single gimbal axis used in precision pointing applications and includes the components listed in Table 1. A brushless DC torque motor serves as the primary (coarse) actuator, while a set of voice coil motors (VCMs) provide the secondary (fine) actuation. The rotation of both the outer and inner axes are measured with a pair of high resolution optical encoders. In the following TISO feedback design example, we assume that only the inner axis measurement is available for feedback. The control algorithms are implemented on an embedded microcontroller with a 1 kHz sample rate.

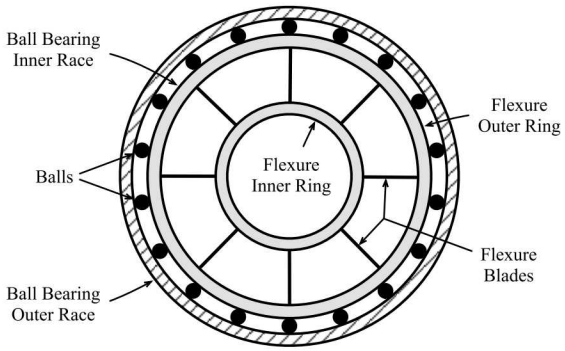

(a) Concept diagram

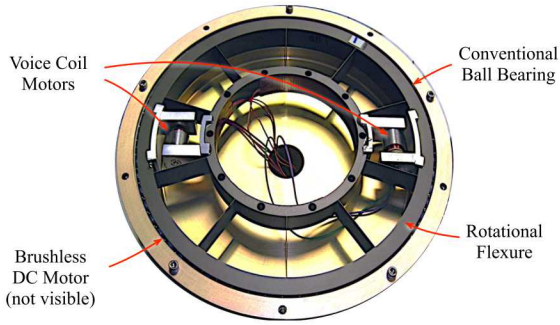

(b) Prototype hardware

Fig. 6 Hybrid flexure bearing

5.2 System model

Neglecting nonlinearities due to bearing friction, the hybrid flexure bearing can be modeled by the simplified two-mass system shown in Fig. 8, where u_1 and u_2 represent the coarse and fine motor torque inputs, y is the measured output, J_1 is the inertia of the outer axis, J_2 is the inertia of the inner axis, b_f is the viscous bearing friction, and k and b are the flexure stiffness and damping, respectively. The TISO plant

Table 1 Testbed components

Component	Manufacturer	Model
Ball Bearings	Kaydon	SA060FZ6Z
Encoder Ring	Renishaw	REXA30USA150B
Encoder Read Head	Renishaw	RA32BAA150B
Brushless DC Motor	Axsys Tech.	BTM-35B
Voice Coil Motor	H2W Tech.	NCC01-04-001-1X

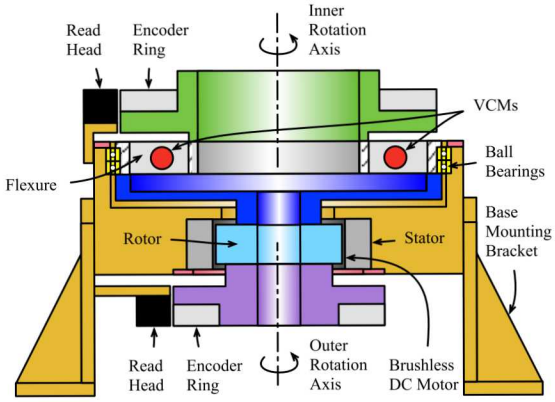

Fig. 7 Experimental testbed

model can then be expressed as $G(s) = \begin{bmatrix} g_1(s) & g_2(s) \end{bmatrix}$ with

$$\begin{aligned} g_1(s) = \frac{Y(s)}{U_1(s)} &= \frac{\frac{b}{J_1 J_2}\left(s + \frac{k}{b}\right)}{s^2\left(s^2 + \frac{b}{J_{\text{eff}}}s + \frac{k}{J_{\text{eff}}}\right) + \frac{b_f}{J_1}s\left(s^2 + \frac{b}{J_2}s + \frac{k}{J_2}\right)} \\ &= \frac{K_1(s + z_1)}{s\,(s + p)\left(s^2 + 2\zeta_p\omega_p s + \omega_p^2\right)} \end{aligned} \tag{33}$$

$$\begin{aligned} g_2(s) = \frac{Y(s)}{U_2(s)} &= \frac{\frac{1}{J_2}s\left(s + \frac{b_f}{J_1}\right)}{s^2\left(s^2 + \frac{b}{J_{\text{eff}}}s + \frac{k}{J_{\text{eff}}}\right) + \frac{b_f}{J_1}s\left(s^2 + \frac{b}{J_2}s + \frac{k}{J_2}\right)} \\ &= \frac{K_2\,(s + z_2)}{(s + p)\left(s^2 + 2\zeta_p\omega_p s + \omega_p^2\right)} \end{aligned} \tag{34}$$

where $J_{\text{eff}} = \frac{J_1 J_2}{J_1 + J_2}$. Using the nominal model parameter values given in Table 2, the transfer function gains, zero/pole locations, natural frequencies, and damping ratios are calculated as

$$\begin{gathered} K_1 = 3.234, \quad K_2 = 1.412, \\ z_1 = 2\pi(3.46 \times 10^3), \quad z_2 = 2\pi(6.03), \\ p = 2\pi(2.58), \quad \omega_p = 2\pi(46.8), \quad \zeta_p = 0.0435 \end{gathered} \tag{35}$$

The plant transfer functions are compared to measured frequency response data in Fig. 9. Overall, the plant model agrees well with the experimental results. Model discrepancies for $g_1(s)$ at higher frequencies (above 200 Hz) are due to unmodeled flexible dynamics.

5.3 Pre-compensator design: Actuator allocation using alignment contours

The first step of the PQ method involves the selection of the pre-compensators, $c_1'(s)$ and $c_2'(s)$, to appropriately allocate the primary (coarse) and secondary (fine) actuators over frequency by shaping the PQ

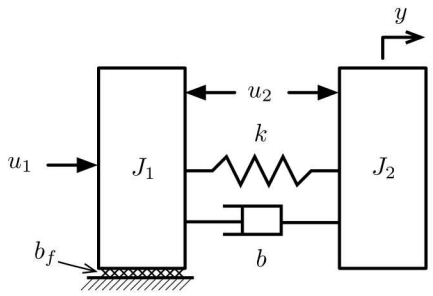

Fig. 8 Simplified 2-DOF model

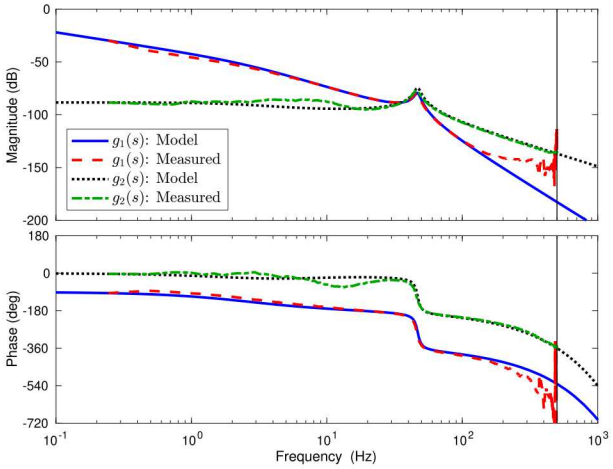

Fig. 9 Plant frequency responses

frequency response. We now show how the alignment contours can be used to assist with this step. For the plant model defined by Eqs. (33) and (34), the plant ratio can be expressed as

$$P(s) = \frac{g_1(s)}{g_2(s)} = \frac{K(s+z_1)}{s\,(s+z_2)} \tag{36}$$

Table 2 Model parameters

Parameter	Symbol	Value	Units
Flexure stiffness	k	26300	in-oz/rad
Flexure damping	b	1.21	in-oz-s/rad
Bearing friction	b_f	20	in-oz-s/rad
Outer axis inertia	J_1	0.528	in-oz-s^2
Inner axis inertia	J_2	0.708	in-oz-s^2

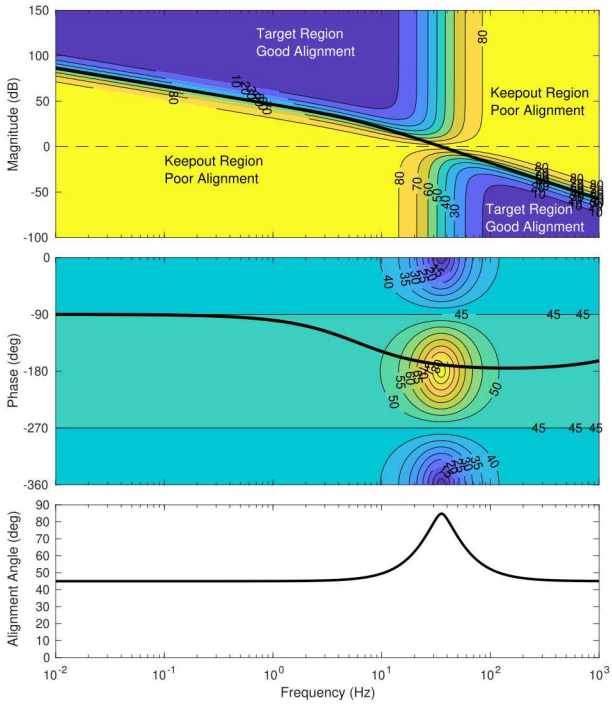

Fig. 10 PQ Bode plot with alignment contours for $Q = 1$

where $K = K_1/K_2$. We can observe the plant's alignment to a unity controller, $C(s) = \begin{bmatrix}1 & 1\end{bmatrix}^T$, by selecting $Q(s) = 1$. Figure 10 shows the Bode plot of PQ with alignment contours drawn for $\phi \in [0°, 90°]$ in $10°$ intervals. The intersections of the magnitude and phase curves with each contour indicate the value of the plant/controller alignment angle at a particular frequency. This can be easily verified with the plot of alignment angle over frequency (using Eq. (9)) at the bottom of Fig. 10. Note that the unity controller is not well aligned with the plant at any frequency ($\phi \geq 45° \; \forall \; \omega$), and is very poorly aligned ($\phi \approx 90°$) near 35 Hz.

The alignment contours represent the level sets of a three-dimensional surface which are viewed from above on the modified PQ Bode plot. The use of color mapped contour regions makes it is easier to distinguish the "peaks" and "valleys" of the surfaces which correspond to large and small alignment angles, respectively. These regions can be used as guidelines for shaping the PQ frequency response to achieve better alignment. As indicated in Fig. 10, it is desirable to target the darker regions where alignment is good ($\phi \approx 0°$) and avoid the lighter regions where alignment is poor ($\phi \approx 90°$). The graphical alignment contours provide valuable insight into the relationship between the PQ loop shape and the plant/controller alignment.

To illustrate the utility of the alignment contours, consider the two different PQ loop shapes shown in Figs. 11 and 12, both of which satisfy the requirements outlined in Sec. 4.1, but have significantly different degrees of plant/controller alignment over frequency. For the sake of comparison, the first design, shown in Fig. 11, is intentionally shaped to yield poor alignment over a wide frequency range. This is accomplished by using a double lead compensator centered about 35 Hz. Although alignment is improved near 35 Hz due to the additional phase lead, the corresponding shift in gain causes the magnitude and phase responses to enter the lighter keepout regions. We can see from the magnitude contours that this is due to inadequate low frequency gain and excessive high frequency gain, resulting in very poor alignment over a large frequency range. According to the results of Sec. 3, we expect large input sensitivities and closed loop interactions for

Design #1.

The second design example, shown in Fig. 12, is shaped to improve the overall plant/controller alignment. This is accomplished with simple compensation techniques to shape the PQ frequency response using the graphical alignment contours as guidelines. An integrator + zero is used to boost the low frequency gain while avoiding additional phase lag at higher frequencies. The integral action bends the magnitude response upward into the darker target region which significantly improves the alignment angle at lower frequencies. A low pass filter provides high frequency roll-off to steer the magnitude response downward into the lower target region which improves alignment at higher frequencies. To satisfy the conditions given in Sec. 4.1, lead compensation is used near the crossover to achieve a phase margin of 60°. Although Design #2 is well aligned at both low and high frequencies, it is not possible to maintain such good alignment over the entire frequency range. This is due to the inherent tradeoff between the alignment angle and phase margin at hand-off. As indicated by the magnitude contours, alignment can be improved with a steeper magnitude response near the crossover. However, due to the Bode gain-phase relationship [28], this comes at the expense of reduced phase margin. Since adequate phase margin is required to avoid destructive interference and NMP zeros, the alignment angle must necessarily increase in the hand-off region. The alignment contours make these tradeoffs clear.

The controller ratios that achieve the PQ loop shapes for the two different designs shown in Figs. 11 and 12 are

$$Q_1(s) = \frac{13.928\,(s+60.27)^2}{(s+839.5)^2} \tag{37}$$

$$Q_2(s) = \frac{2834.4\,(s+94.25)\,(s+39.88)\left(s^2+237.1s+2.87\times10^4\right)}{s\,(s+1283)\,(s+314.2)\,(s^2+377.2s+7.26\times10^4)} \tag{38}$$

It is straightforward to select the pre-compensators c_1' and c_2' through the relationship defined in Eq. (26). Since Q is realizable, a reasonable choice is to select $c_1' = Q$ and $c_2' = 1$. Figure 13 shows the Bode plot of $G_{\text{SISO}} = c_1' g_1 + c_2' g_2$ for the two designs.

5.4 Post-compensator design: Output equivalent controllers

The second step of the PQ method involves the selection of the post-compensator, $c_0(s)$, to satisfy stability and performance requirements. In order to make fair comparisons of closed loop performance, we must choose the post-compensators for the two designs such that they achieve identical output responses. This ensures that any differences in closed loop performance at the plant input can be solely attributed to differences in plant/controller alignment.

Because the plant G, defined in Eq. (1), has a non-trivial right nullspace, it follows that there are many choices of the controller C that yield the same fixed set of output transfer functions [9], denoted as L_O^*, S_O^*, and T_O^*. This set of controllers is defined as

$$\mathcal{C}(L_O^*(j\omega)) \coloneqq \{C(j\omega) : G(j\omega)C(j\omega) = L_O^*(j\omega)\} \tag{39}$$

where any $C(j\omega) \in \mathcal{C}(L_O^*(j\omega))$ is called an *output equivalent controller* [9].

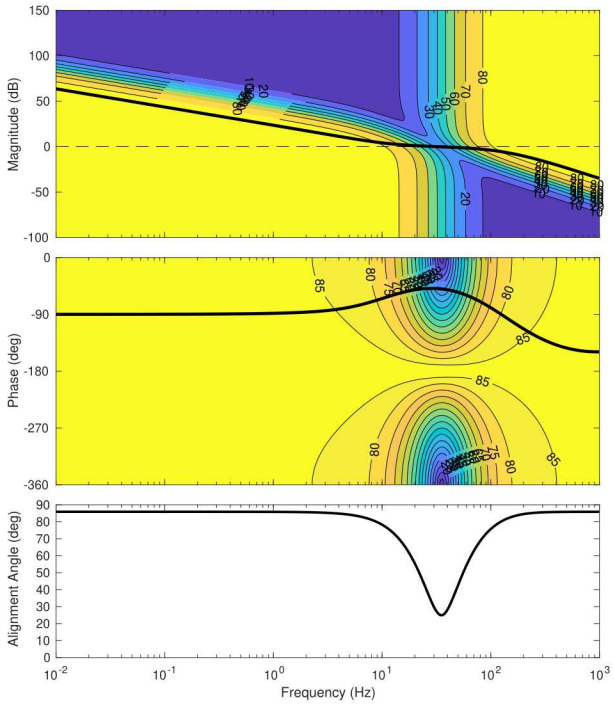

Fig. 11 PQ Bode plot for Design #1

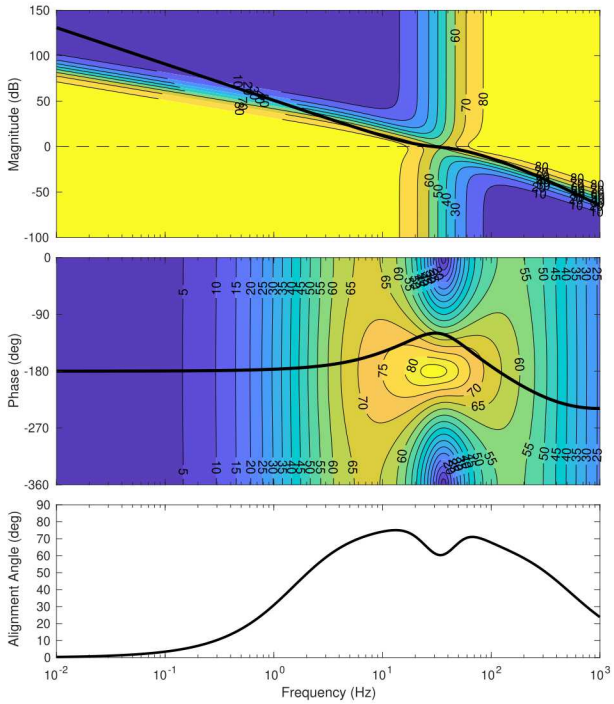

Fig. 12 PQ Bode plot for Design #2

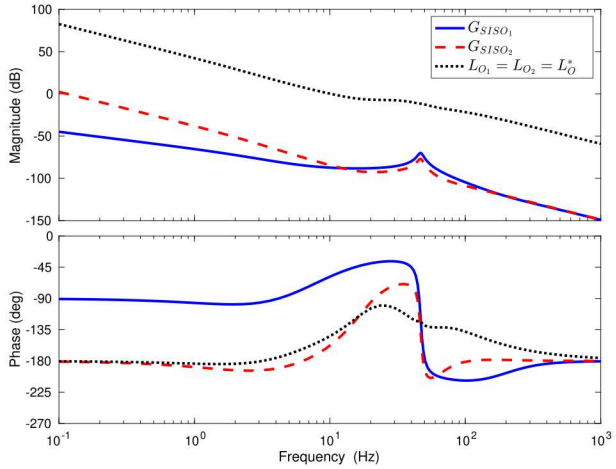

Fig. 13 Bode plot of G_{SISO} and L_O

Let C_1 and C_2 be the controllers for Design #1 and Design #2, respectively. To obtain output equivalent controllers such that $C_1, C_2 \in \mathcal{C}(L_O^*)$, we first select the post-compensator for Design #2 to achieve a crossover frequency of 10 Hz with a phase margin of 35° and a gain margin of at least 6 dB. This is achieved with a cascaded lead compensator and notch filter given by

$$c_{0_2} = \frac{30801\,(s+36.28)\left(s^2+25.92s+8.61\times10^4\right)}{(s+108.8)\left(s^2+410.8s+8.61\times10^4\right)} \tag{40}$$

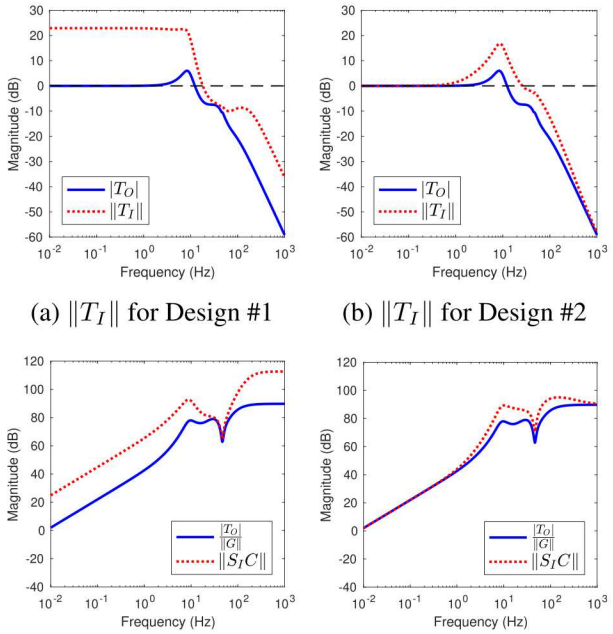

(a) $\|T_I\|$ for Design #1 (b) $\|T_I\|$ for Design #2

(c) $\|S_I C\|$ for Design #1 (d) $\|S_I C\|$ for Design #2

Fig. 14 Comparison of input sensitivities

Figure 13 shows the Bode plot of $L_{O_2} = GC_2 = c_{0_2} G_{\text{SISO}_2}$. To ensure that $C_1 \in \mathcal{C}(L_O^*)$ such that $GC_1 = GC_2 = L_O^*$, the post-compensator for Design #1 must satisfy

$$c_{0_1} = \frac{L_O^*}{G_{\text{SISO}_1}} \tag{41}$$

6 RESULTS

Figure 14 compares $\|T_I\|$ and $\|S_I C\|$ for the two designs obtained in the previous section. The plots of $|T_O|$ and $|T_O|/\|G\|$ are also included, which represent the minimum possible value of $\|T_I\|$ and $\|S_I C\|$ in the case of perfect alignment according to Eqs. (21) and (22), respectively. Note that $|T_O|$ and $|T_O|/\|G\|$ are identical for both designs through the use of output equivalent controllers.

Figure 14(a) shows the plot of $\|T_I\|$ for Design #1. We see that $\|T_I\|$ has a large DC gain, which is due to the poor plant/controller alignment at low frequency. This will ultimately result in a large closed loop response to input disturbances. On the other hand, we see that $\|T_I\|$ has a unity DC gain for Design #2 shown in Fig. 14(b). This is a direct result of the nearly perfect alignment achieved at low frequencies in Design #2. To illustrate the effect of alignment on the closed loop interactions at the plant input, we compare the DC gain matrix, $T_I(0)$, for each design:

$$\text{Design \#1:} \quad T_I(0) = \begin{bmatrix} 1 & 0 \\ 13.9 & 0 \end{bmatrix}$$

$$\text{Design \#2:} \quad T_I(0) = \begin{bmatrix} 1 & 0 \\ 0 & 0 \end{bmatrix}$$

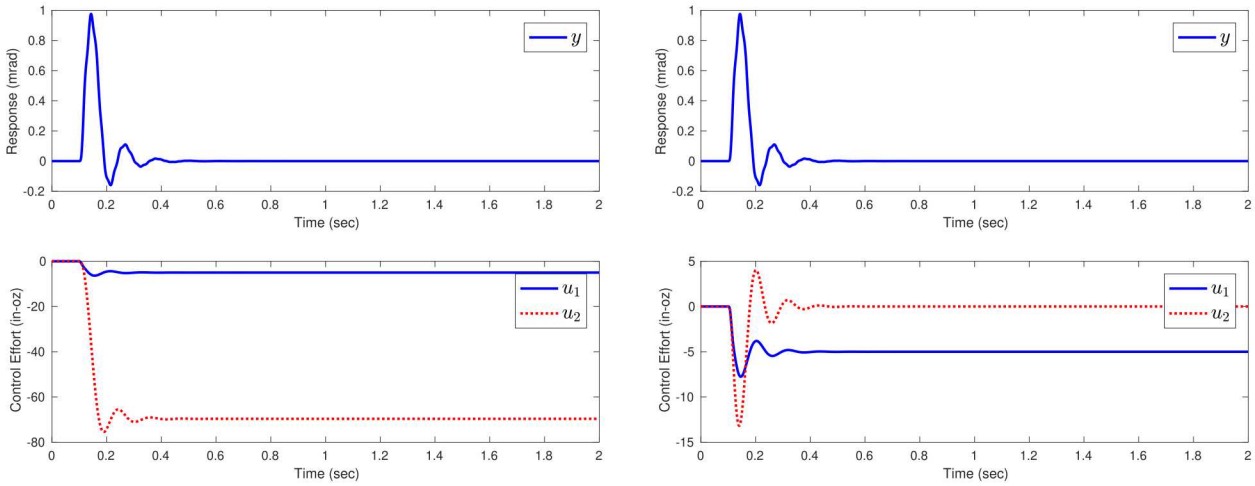

(a) Input disturbance response for Design #1

(b) Input disturbance response for Design #2

Fig. 15 Comparison of input disturbance responses

Due to poor low frequency alignment, Design #1 produces a large off-diagonal term creating a significant one-way interaction between $d_{i1} \rightarrow u_2$ at the plant input. On the other hand, Design #2 produces no interactions due to perfect alignment at $\omega = 0$.

The simulated closed loop responses to a step input disturbance, $D_I = \begin{bmatrix} 5 & 0 \end{bmatrix}^T$, are compared in Fig. 15. Note that the output response, y, for each design is identical due to the use of output equivalent controllers. However, the input responses, u_1 and u_2, are drastically different. As shown in Fig. 15(a), Design #1 produces a large control response on the second controller output, u_2. This is undesirable in practice since the saturation limits of the secondary actuator are typically much smaller than the primary actuator. Indeed, Design #1 exceeds the saturation limits of the VCMs, which only provide a maximum torque capability of 16.1 in-oz. As shown in Fig. 15(b), Design #2 produces a well-behaved control response which avoids actuator saturation. This is due to the improved alignment at low frequency, hence smaller $\|T_I\|$ and reduced interactions.

Similarly, the effects of alignment on $\|S_I C\|$ for the two different designs are shown in Figs. 14(c) and 14(d). We see that elevated values of $\|S_I C\|$ occur at frequencies where alignment is poor. Design #1 produces large $\|S_I C\|$ over a wide frequency range where alignment is poor. Design #2 overall reduces $\|S_I C\|$ where alignment is improved. The simulated closed loop responses to reference step commands are compared in Fig. 16. Although the output response, y, for each design is identical, the input responses, u_1 and u_2, are again quite different. As shown in Fig. 16(a), Design #1 exhibits a very large transient response on the primary actuator. In this case, u_1 exceeds the DC motor's maximum torque capability of 81.3 in-oz. This large transient is due to poor alignment at high frequency which forces $\|S_I C\|$ to be large. As shown in Fig. 16(b), Design #2 reduces the control transients and avoids actuator saturation as a result of the improved alignment at high frequency.

7 EXPERIMENTAL VALIDATION

The two controller designs obtained in Sec. 5 were discretized using the bilinear (Tustin) approximation and implemented on the experimental testbed with a 1 kHz sample rate. Figure 17 compares the experimental step responses for the two designs. Due to friction, the measured responses are more highly damped

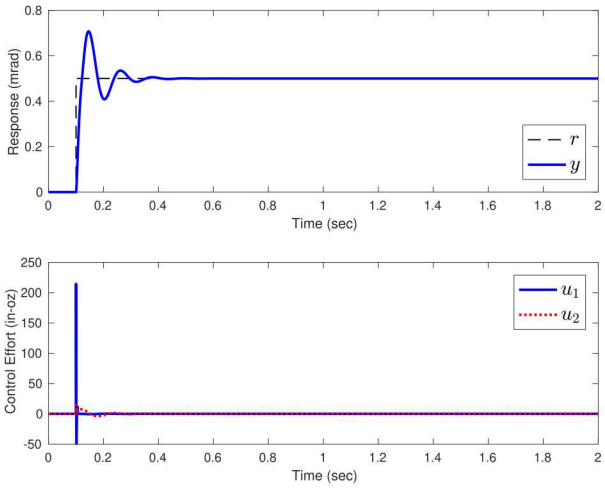

(a) Step response for Design #1

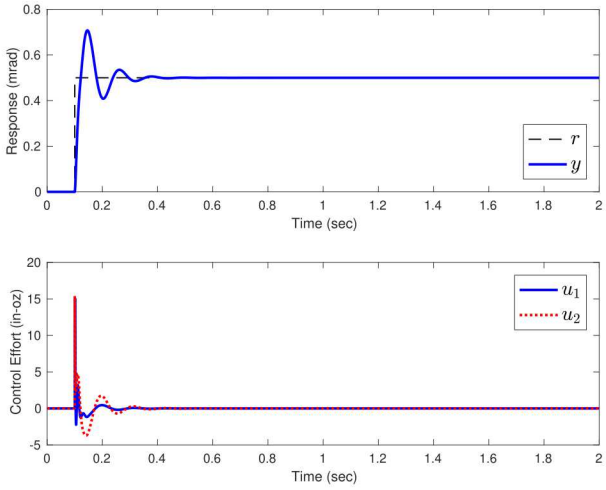

(b) Step response for Design #2

Fig. 16 Comparison of step responses

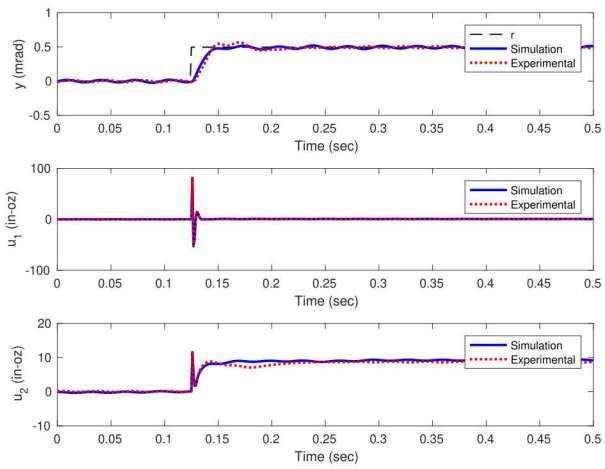

(a) Experimental step response for Design #1

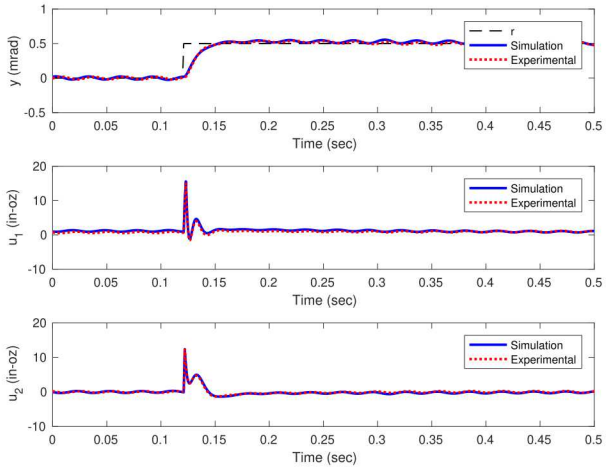

(b) Experimental step response for Design #2

Fig. 17 Comparison of experimental step responses

than the ideal linear responses shown in Fig. 16. Thus, the measured responses are compared with results obtained from a higher fidelity model which includes actuator saturation and dynamic friction [25]. The simulated responses are in good agreement with the experimental results. As shown in Fig. 17(a), the poor alignment of Design #1 causes a large transient response on the primary actuator and causes it to saturate. The improved alignment of Design #2 reduces the transient response so that neither actuator saturates, as shown in Fig. 17(b).

8 CONCLUSIONS

This paper presents a graphical controller design approach which explicitly accounts for plant/controller alignment in the design process. This approach, which is an extension to the PQ method [1], allows the

designer to easily determine the alignment angle over frequency through graphical alignment contours on the PQ Bode plot. It provides the designer with valuable insights into desirable loop shapes that yield well-aligned controllers for a given plant, thereby minimizing closed loop sensitivity and closed loop interactions at the plant input. The approach also indicates regions where alignment must be necessarily poor due to inherent limitations dictated by the plant.

ACKNOWLEDGEMENTS

The authors would like to thank R. Rosenthal for his assistance with the experimental testbed. Financial support for this research effort was provided by Sandia National Laboratories. Sandia is a multi-mission laboratory managed and operated by National Technology and Engineering Solutions of Sandia, LLC, a wholly owned subsidiary of Honeywell International, Inc., for the U.S. Department of Energy's National Nuclear Security Administration under contract DE-NA-0003525. This paper describes objective technical results and analysis. Any subjective views or opinions that might be expressed in the paper do not necessarily represent the views of the U.S. Department of Energy or the United States Government.

REFERENCES

[1] S. J. Schroeck, W. C. Messner, and R. J. McNab, "On compensator design for linear time-invariant dual-input single-output systems," *IEEE/ASME Transactions on Mechatronics*, vol. 6, pp. 50–57, Mar. 2001.

[2] W. S. Nagel, G. M. Clayton, and K. K. Leang, "Master-slave control with hysteresis inversion for dual-stage nanopositioning systems," in *Proceedings of the American Control Conference*, (Boston, MA), July 2016.

[3] U. Boettcher, B. Raeymaekers, R. A. de Callafon, and F. E. Talke, "Dynamic modeling and control of a piezo-electric dual-stage tape servo actuator," *Transactions on Magnetics*, vol. 45, pp. 3017–3024, July 2009.

[4] M. Stalder, Y. Michellod, P. Mullhaupt, and D. Gillet, "Dedicated controller design for a dual-stage opto-mechatronic system," in *Proceedings of the IEEE/ASME International Conference on Advanced Intelligent Mechatronics*, (Xi'an, China), July 2008.

[5] E. D. Miller and R. A. de Callafon, "Dual-stage servo control for an optical pointing system," in *Proceedings of the ASME Information Storage and Processing Systems Conference*, (Santa Clara, CA), June 2013.

[6] Z. Wu, X. Chen, W. Hua, and J. Wang, "Design of coarse-fine control system for wafer stage of lithography using PQ method," in *Proceedings of ISSCAA*, (Harbin, China), June 2010.

[7] P. Gorzelic, E. Hellström, A. Stefanopoulou, L. Jiang, and S. Gopinath, "A coordinated approach for throttle and wastegate control in turbocharged spark ignition engines," in *Proceedings of the Chinese Control and Decision Conference*, (Taiyuan, China), May 2012.

[8] S. Brennan and A. Alleyne, "Integrated vehicle control via coordinated steering and wheel torque inputs," in *Proceedings of the American Control Conference*, (Arlington, VA), June 2001.

[9] J. Freudenberg and R. Middleton, "Properties of single input, two output feedback systems," *International Journal of Control*, vol. 72, no. 16, pp. 1446–1465, 1999.

[10] J. Freudenberg and R. Middleton, "Design rules for multivariable feedback systems," in *Proceedings of the IEEE Conference on Decision and Control*, (Kobe, Japan), pp. 1980–1985, Dec. 1996.

[11] J. S. Freudenberg and A. Y. Karnik, "Reverse engineering a multivariable controller: A case study," in *Proceedings of the American Control Conference*, (Portland, OR), pp. 733–738, June 2005.

[12] M. Kerr, C.-Y. Lan, and S. Jayasuriya, "Control of two-input two-output systems exploiting alignment," in *Proceedings of the IEEE Conference on Decision and Control*, (San Diego, CA), pp. 4393–4398, Dec. 2006.

[13] K. Zhou, J. C. Doyle, and K. Glover, *Robust and Optimal Control*. Upper Saddle River, NJ: Prentice Hall, 1996.

[14] A. R. Woodyatt, J. S. Freudenberg, and R. H. Middleton, "An integral constraint for single input two output feedback systems," *Automatica*, vol. 37, no. 11, pp. 1717–1726, 2001.

[15] M. M. Seron, J. H. Braslavsky, and G. C. Goodwin, *Fundamental Limitations in Filtering and Control*. London: Springer-Verlag, 1997.

[16] A. Saberi and P. Sannuti, "Squaring down by static and dynamic compensators," *IEEE Transactions on Automatic Control*, vol. 33, pp. 358–365, Apr. 1988.

[17] E. J. Davison, "Some properties of minimum phase systems and 'squared-down' systems," *IEEE Transactions on Automatic Control*, vol. 28, pp. 221–222, Feb. 1983.

[18] W. Messner, "Some advances in loop shaping controller design with applications to disk drives," *IEEE Transactions on Magnetics*, vol. 37, pp. 651–656, Mar. 2001.

[19] S. C. Smith and W. Messner, "Loop shaping with closed-loop magnitude contours on the Bode plot," in *Proceedings of the American Control Conference*, (Anchorage, AK), May 2002.

[20] L. Xia and W. Messner, "An improved version of the RBode plot," in *Proceedings of the American Control Conference*, (Seattle, WA), June 2008.

[21] T. Atsumi and W. C. Messner, "Modified Bode plots for robust performance in SISO systems with structured and unstructured uncertainties," *IEEE Transactions on Control Systems Technology*, vol. 20, pp. 356–368, Mar. 2012.

[22] J. M. Hilkert, "Inertially stabilized platform technology: Concepts and principles," *IEEE Control Systems Magazine*, vol. 28, pp. 26–46, Feb. 2008.

[23] P. S. Barney, N. A. Weir, and R. R. Rosenthal, "Combination bearing/flexure joint for large coarse motions and fine jitter control," Tech. Rep. SAND2014-19413, Sandia National Laboratories, Albuquerque, NM, Oct. 2014.

[24] T. E. Salas, P. S. Barney, A. M. Ison, R. L. Akau, and N. Weir, "Rotation flexure with temperature controlled modal frequency." U.S. Patent 9,759,263, Sept. 2017.

[25] N. A. Weir and A. G. Alleyne, "An improved dynamic friction model using a data-based approach," in *Proceedings of the ASME Dynamic Systems and Control Conference*, (Tysons, VA), Oct. 2017.

[26] N. A. Weir and A. G. Alleyne, "Controller design for two-input single-output systems exploiting plant/controller alignment," in *Proceedings of the ASME Dynamic Systems and Control Conference*, (Atlanta, GA), Oct. 2018.

[27] T. E. Salas, P. S. Barney, A. M. Ison, R. L. Akau, and N. Weir, "Rotation flexure with temperature controlled modal frequency." U.S. Patent 10,288,121, May 2019.

[28] H. W. Bode, *Network Analysis and Feedback Amplifier Design*. New York: D. Van Nostrand Company, 1945.

LIST OF FIGURES

1 TISO feedback system . . . 3
2 PQ equivalent representation . . . 8
3 PQ feedback system . . . 8
4 PQ Bode plot . . . 9
5 Gimbaled pointing system . . . 11
6 Hybrid flexure bearing . . . 12
7 Experimental testbed . . . 13
8 Simplified 2-DOF model . . . 14
9 Plant frequency responses . . . 14
10 PQ Bode plot with alignment contours for $Q = 1$ . . . 15
11 PQ Bode plot for Design #1 . . . 17
12 PQ Bode plot for Design #2 . . . 17
13 Bode plot of G_{SISO} and L_O . . . 17
14 Comparison of input sensitivities . . . 18
15 Comparison of input disturbance responses . . . 19
16 Comparison of step responses . . . 20
17 Comparison of experimental step responses . . . 20

LIST OF TABLES

1 Testbed components 12
2 Model parameters 14